Manuscript prepared for Atmos. Chem. Phys. Discuss.
with version 2014/07/09 7.01 Copernicus papers of the LaTeX class copernicus.cls.
Date: 25 March 2015

The 11-year solar cycle in current reanalyses: A (non)linear attribution study of the middle atmosphere~~Solar cycle in current reanalyses: (non)linear attribution study~~[ales](r4,tc3;r2,sc1)

Ales Kuchar[1], **Petr Sacha**[1], **Jiri Miksovsky**[1], **and Petr Pisoft**[1]

[1]Department of Atmospheric Physics, Faculty of Mathematics and Physics, Charles University in Prague, V Holesovickach 2, 180 00 Prague 8, Czech Republic

Correspondence to: A. Kuchar (kuchara@mbox.troja.mff.cuni.cz)

Abstract

This study focusses on the variability of temperature, ozone and circulation characteristics in the stratosphere and lower mesosphere with regard to the influence of the 11-year solar cycle. It is based on attribution analysis using multiple nonlinear techniques (Support Vector Regression, Neural Networks) besides the multiple linear regression~~traditional linear~~[ales](r4,tc4) approach. The analysis was applied to several current reanalysis datasets for the 1979-2013 period, including MERRA, ERA-Interim and JRA-55, with the aim to compare how this type of data resolves especially the double-peaked solar response in temperature and ozone variables and the consequent changes induced by these anomalies. Equatorial temperature signals in the lower and upper stratosphere were found to be sufficiently robust and in qualitative agreement with previous attribution~~observational~~[ales](r4,sc29) studies. The analysis also pointed to the solar signal in the ozone datasets (i.e. MERRA ERA-Interim) not being consistent with the observed double-peaked ozone anomaly extracted from satellite measurements. Consequently the results obtained by linear regression were confirmed by the nonlinear approach through all datasets, suggesting that linear regression is a relevant tool to sufficiently resolve the solar signal in the middle atmosphere. Furthermore, the seasonal evolution of the solar response was also discussed in terms of dynamical causalities in the winter hemispheres~~the seasonal dependence of the solar response was also discussed, mainly as a source of dynamical causalities in the wave propagation characteristics in the zonal wind and the induced meridional circulation in the winter hemispheres~~[ales](r3,c6). The hypothetical mechanism of a weaker Brewer Dobson circulation at solar maxima[ales](r3,c6) was reviewed together with discussion of polar vortex behaviour~~stability~~[ales](r4,sc25).

1 Introduction

The Sun is a prime driver of various processes in the climate system. From observations of the Sun's variability on decadal or centennial time scales, it is possible to identify temporal

patterns and trends in solar activity, and consequently to derive the related mechanisms of the solar influence on the Earth's climate (e.g. Gray et al., 2010). Of the semi-regular solar cycles, the most prominent is the approximate 11-year periodicity which manifests in the solar magnetic field or through fluctuations of sunspot number, but also in the total solar irradiance (TSI) or solar wind properties. For the dynamics of the middle atmosphere, where most of[ales](r2,sc2) ozone production and destruction occurs, the changes in the spectral solar irradiance (SSI) are the most influential, since the TSI as the integral over all wavelengths exhibits variations of orders lower than the ultraviolet part of the spectrum (Lean, 2001). This fact was supported by original studies (e.g. Labitzke, 1987; Haigh, 1994) that suggested the solar cycle influence on the variability of the stratosphere. Gray et al. (2009) have shown, with the fixed dynamical heating model, that the response of temperature in the photochemically controlled region of the upper tropical[ales](r3,c7) stratosphere is approximately given 60% by direct solar heating and 40% due to indirect effect by the ozone changes.

Numerous ~~observational~~[ales](r4,sc29) studies have identified temperature and ozone changes linked to the 11-year cycle by multiple linear regression. The use of ERA-40 reanalysis (Frame and Gray, 2010) pointed to a manifestation of annually averaged solar signal in temperature, exhibit~~ed~~[ales] predominantly around the equator with amplitudes up to 2 K around the stratopause and with a secondary amplitude maximum of up to 1 K in the lower stratosphere. Soukharev and Hood (2006), Hood et al. (2010) and Randel and Wu (2007) have used satellite ozone data sets to characterize statistically significant responses in the upper and lower stratosphere. The observed double-peaked ozone anomaly in the vertical profile around the equator was reproduced, nevertheless the concerns about physical mechanism of the lower stratospheric response was expressed (Austin et al., 2008).~~The observed double-peaked ozone anomaly in the vertical profile around the equator was confirmed by the simulations of coupled chemistry climate models (Austin et al., 2008).~~[ales](r3,c3,c8)

The ozone and temperature perturbations associated with the solar cycle have an impact on the middle atmospheric circulation. They produce a zonal wind anomaly around the stratopause (faster subtropical jet) during solar maxima through the enhanced merid-

ional temperature gradient. Since planetary wave propagation is affected by the zonal mean flow (Andrews and McIntyre, 1987), we can suppose that a stronger subtropical jet can deflect planetary waves propagating from higher latitudes. Reduced wave forcing can lead to decreasing/increasing and or upwelling/downwelling motions in the equatorial or higher latitudes respectively (Kodera and Kuroda, 2002). The Brewer-Dobson circulation (BDC) is weaker during solar maxima (Kuroda and Kodera, 2001)~~(Gray et al., 2010)~~[ales](r2,s6) although this appears to be sensitive to the state of the polar winter. Observational studies, together with model experiments (e.g. Matthes et al., 2006) suggest a so-called "Top-Down" mechanism where the solar signal is transferred from the upper to lower stratosphere, and even to tropospheric altitudes.

Statistical studies (e.g. Labitzke et al., 2006; Camp and Tung, 2007) have also focused on the lower stratospheric solar signal in the polar regions and have revealed modulation by the Quasi-biennial oscillation (QBO), or the well known Holton-Tan relationship (Holton and Tan, 1980) modulated by the solar cycle. Proposed mechanisms by Matthes et al. (2004, 2010)[ales](r2,sc4) suggested that the solar signal induced during early winter in the upper equatorial stratosphere propagates poleward and downward when the stratosphere transits from a radiatively controlled state to a dynamically controlled state involving planetary wave propagation (Kodera and Kuroda, 2002). The mechanism of the solar cycle and QBO interaction, which stems from reinforcing each other or canceling each other out (Gray et al., 2004) has been verified by WACCM3.1~~recent~~[ales] model simulations (Matthes et al., 2013). These proved the independence of the solar response in the tropical upper stratosphere from the response dependent on the presence of the QBO in lower altitudes. However, fully coupled WACCM-4 model simulations by Kren et al. (2014) raised the possibility of occurrence of the observed solar-QBO response in the polar region.[ales](r2,sc5)

~~Observational and modeling studies over the past two decades have fundamentally changed our understanding of wave processes and the coupling between the middle atmosphere and tropospheric conditions (**?**). It has been shown that the stratosphere plays a significant and active role in tropospheric circulation on various time scales (**???**). A deeper understanding of the mechanisms of communication between the middle atmosphere and troposphere~~

~~contributes to better climate change predictions. However, a number of questions about the coupling processes with regard to solar signal perturbation have to be answered.~~[ales](r4,sc2)
It has been shown that difficulties in the state-of-the-art climate models arise when reproducing the solar signal influence on winter polar circulation, especially in less active sun periods (Ineson et al., 2011). The hypothesis is that solar UV forcing is too weak in the models. Satellite measurements indicate that variations in the solar UV irradiance may be larger than previously thought (Harder et al., 2009). However, the measurements by Harder et al. (2009) from SORCE satellite may have been affected by instrument degradation with time and so may be overestimated in the UV (Ermolli et al., 2013). They have also concluded that the SORCE measurements probably represent the upper limit in the magnitude of the SSI variation. Consequent results of GCMs, forced with the SSI from the SORCE measurements, have shown larger stratospheric response than for NRLSSI dataset. Thus, coordinated work is needed to have reliable SSI input data for GCM simulations (Ermolli et al., 2013), and also to propose robust conclusions concerning solar cycle (SC) influence on climate (Ball et al., 2014).[ales](r3,c9;r4,sc3)

At the Earth's surface, the detection of the solar cycle influence is problematic since there are other significant forcing factors, e.g. greenhouse gases, volcanoes and aerosol changes (e.g. Chiodo et al., 2012)~~(Gray et al., 2010)~~[ales](r2,sc8), as well as substantial variability attributable to internal climate dynamics. However several studies (van Loon et al., 2007; van Loon and Meehl, 2008; Hood and Soukharev, 2012; Hood et al., 2013; Gray et al., 2013; Scaife et al., 2013)~~(van Loon et al., 2007; van Loon et al., 2008; van Loon et al., 2012; van~~ detected the solar signal in sea level pressure or sea surface temperature which supports the hypothesis of a troposphere-ocean response to the solar cycle. The studies (e.g. Hood and Soukharev, 2012) suggest a so-called "Bottom-Up" solar forcing mechanism ~~t. T~~[ales](r3,c10)hat contributes to the lower ozone and temperature anomaly in connection with the lower stratosphere deceleration of the BDC. However, the results presented by Chiodo et al. (2014) suggest the contribution of solar cycle variability could be smaller since two major volcanic eruptions are aligned with solar maximum periods and also given the shortness of analysed time series (in our case 35 years). These concerns related to the lower

stratospheric response of ozone and temperature derived from observations has already been raised (e.g. Solomon et al., 1996; Lee and Smith, 2003). However, another issue is whether or not the lower stratospheric response could depend on the model employed in the simulations (Mitchell et al., 2015).[ales](r2,sc8;r4,sc17;r3,c3)

The observed double-peaked ozone anomaly in the vertical profile around the equator was confirmed by the simulations of coupled chemistry climate models (Austin et al., 2008).

Several past studies (e.g. Soukharev and Hood, 2006; Frame and Gray, 2010; Gray et al., 2013; Mitchell et al., 2014a)~~(e.g. Soukharev and Hood, 2006; , 2010; , 2013)~~[ales](r2,sc11+c1) used multiple linear regression to extract the solar signal and separate other climate phenomena like the QBO, the effect of aerosols, NAO, ENSO or trend variability. Apart from this conventional method, it is possible to use alternative approaches to isolate and examine particular signal components, such as wavelet analysis (Pisoft et al., 2012, 2013) or empirical mode decomposition (Coughlin and Tung, 2004). The nonlinear character of the climate system also suggests potential benefits from the application of ~~alternative,~~[ales] full nonlinear attribution techniques to study of properties and interactions in the atmosphere. However, such nonlinear ~~methods~~techniques[ales] have been used rather sporadically in the atmospheric sciences (e.g. Walter and Schönwiese, 2003; Pasini et al., 2006; Blume and Matthes, 2012), mainly due to their several disadvantages such as the lack of explanatory power (Olden and Jackson, 2002).

To examine middle atmospheric conditions, it is necessary to study reliable and sufficiently vertically resolved data. Systematic and global observations of the middle atmosphere only began during the International Geophysical Year (1957-1958) and were later expanded through the development of satellite measurements (Andrews and McIntyre, 1987). Supplementary data come from balloon and rocket soundings, though these are limited by their vertical range (only the lower stratosphere in the case of radiosondes) and the fact that the in situ observations measure local profiles only. By assimilation of these irregularly distributed data and discontinuous measurements of particular satellite missions into an atmospheric/climatic model, we have modern basic datasets available for climate research, so called reanalyses. These types of data are relatively long, glob-

ally gridded with a vertical range extending to the upper stratosphere or the lower mesosphere and thus suitable for 11-year solar cycle research. In spite of their known limitations (such as discontinuities in ERA reanalysis – McLandress et al., 2013), they are considered an extremely valuable research tool (Rienecker et al., 2011). Coordinated intercomparison has been initiated by the SPARC community to understand current reanalysis products, and to contribute to future reanalysis improvements (Fujiwara et al., 2012). Under this framework the paper by Mitchell et al. (2014a) has been published where 9 reanalysis datasets were examined in terms of 11-year SC, volcanic, ENSO and QBO variability. Complementing their study, we provide comparison with nonlinear regression techniques here, assessing robustness of the results obtained by Multiple Linear Regression (MLR). Furthermore, EP-flux diagnostics are used to examine solar-induced response during winter season in both hemispheres, and solar-related variations of assimilated ozone are investigated.[ales](r1,c1;r2,sc11+c1;r3,c5;r4,c4)

The paper is arranged as follows. In section 2 the used datasets are described. In section 3 the analysis methods are presented along with regressor terms employed in the regression model. Section 4 is dedicated to the description of the annual response results. In subsection 4.1.1 solar response in MERRA reanalysis is presented. Next, in subsection 4.1.2 other reanalyses are compared in terms of SC. Comparison of linear and nonlinear approaches is presented in subsection 4.1.3. Section 4.3. describes monthly evolution of SC response in the state variables. Section 5 is aimed at dynamical consequences of the SC analysed using the EP-flux diagnostics.[ales](r4,sc4)

2 Datasets

Our analysis was applied to the most recent generation~~to the last generation~~[ales](r2,sc12) of three reanalysed datasets: MERRA (Modern Era Reanalysis for Research and Applications, developed by NASA) (Rienecker et al., 2011), ERA-Interim (ECMWF Interim Reanalysis) (Dee et al., 2011) and JRA-55 (Japanese 55-year Reanalysis) (Ebita et al., 2011). We have studied the series for the period 1979-2013. All of the datasets were analysed

on a monthly basis. The Eliassen–Palm (EP) flux diagnostics (described below) was computed on a 3-hourly basis from MERRA reanalysis and subsequently monthly means were produced. Similar approach has been already used by Seviour et al. (2012) and Mitchell et al. (2014b). The former study proposed that even 6-hourly data are not only necessary but should also be sufficient to diagnose tropical upwelling in the lower stratosphere.~~The Eliassen–Palm (EP) flux diagnostics (described below) was analysed on the daily basis and subsequently monthly averages were produced.~~[ales](r2,c2,sc13;r4,tc1;r3,c11) The vertical range extends to the lower mesosphere (0.1 hPa) for MERRA, and to 1 hPa for the remaining reanalyses[ales]. The horizontal resolution of the gridded datasets was 1.25°x1.25° for MERRA and JRA-55 and 1.5°x1.5° for ERA-Interim respectively.

In comparison with previous generations of reanalyses~~reanalysis~~[ales], it is possible to observe a better representation of stratospheric conditions. This improvement is considered to be connected with increasing the height of the upper boundary of the model domain (Rienecker et al., 2011). For example, ~~T~~[ales](r3,c11)he Brewer-Dobson circulation was markedly overestimated by ERA-40, an improvement was achieved in ERA-Interim, but the upward transport remains faster than observations indicate (Dee et al., 2011). Interim results of JRA-55 suggest a less biased reanalysed temperature in the lower stratosphere relative to JRA-25 (Ebita et al., 2011). In addition to~~Except for~~[ales](r3,c11) the standard variables provided in reanalysis, i.e. air temperature, ozone mixing ratio and circulation characteristics – zonal, meridional or omega velocity, we have also analysed other dynamical variables. Of particular interest were the EP flux diagnostics - a theoretical framework to study interactions between planetary waves and the zonal mean flow (Andrews and McIntyre, 1987). Furthermore, this framework allows the study of the wave propagation characteristics in the zonal wind and the induced (large scale) meridional circulation as well. For this purpose the quasi-geostrophic approximation of Transformed Eulerian Mean (TEM) equations were used in the form employed by Edmon Jr et al. (1980), i.e. using their formula (3.1) for EP flux vectors, (3.2) for EP flux divergence and (3.4) for residual circulation. These variables were then interpolated to a regular vertical grid. For the visualization purposes the EP flux arrows were also scaled via the formula (3.13) in (Ed-

mon Jr et al., 1980). The script was publicly released (Kuchar, 2015).~~For this purpose the quasi-geostrophic approximation of Transformed Eulerian Mean (TEM) equations was used, in the form employed by (Edmon Jr et al., 1980).~~[ales](r2,c2,sc13;r4,tc1)

3 Methods

To detect variability and changes due to climate-forming~~external climate~~[ales] factors, such as the 11-year solar cycle, we have applied an attribution analysis based on Multiple Linear Regression (MLR) and two nonlinear techniques. The regression model separates the effects of climate phenomena that are supposed to have an impact on middle atmospheric conditions. Our regression model of a particular variable X as a function of time t, pressure level p, latitude φ and longitude λ[ales](r4,sc5) is described by the following equation:

$$\begin{aligned} X(t,z,\varphi,\lambda) = &\sum_{i=1}^{12} \alpha_i(z,\varphi,\lambda) + \beta(z,\varphi,\lambda)\,t + \gamma(z,\varphi,\lambda)\,\mathrm{SOLAR}(t) + \delta_1(z,\varphi,\lambda)\,\mathrm{QBO}_1(t) \\ &+ \delta_2(z,\varphi,\lambda)\,\mathrm{QBO}_2(t) + \delta_3(z,\varphi,\lambda)\,\mathrm{QBO}_3(t) + \epsilon(z,\varphi,\lambda)\,\mathrm{ENSO}(t) \\ &+ \zeta(z,\varphi,\lambda)\,\mathrm{SAOD}(t) + \eta(z,\varphi,\lambda)\,\mathrm{NAO}(t) + e(t,z,\varphi,\lambda). \end{aligned} \tag{1}$$

After deseasonalizing which can be represented by α_i indices for every month in a year, the individual terms represent~~we have applied~~[ales](r2,sc14) a trend regressor t either in linear form or including the Equivalent Effective Stratospheric Chlorine (EESC) index (this should be employed due to the ozone turnover trend around the middle of the 90s), ~~t. T~~[ales](r2,sc14)he solar cycle ~~is~~[ales] represented by the 10.7 cm radio flux as a proxy for solar ultraviolet variations at wavelengths 200-300 nm that are important for ozone production and radiative heating in the stratosphere, and[ales](r3,c14) which correlates well with sunspot number variation (the data were acquired from Dominion Radio Astrophysical Observatory (DRAO) in Penticton, Canada).

We have also[ales] included the quasi-biennial proxies as another stratosphere-related predictor. Similar studies have represented the QBO in multiple regression methods in several

ways. Our approach involves three separate QBO indices extracted from the eachMERRA[ales](r4,sc reanalysis. These three indices are the first three principal components of the residuals of our linear regression model (1) excluding QBO predictors applied to the equatorial zonal wind. The approach follows the paper by Frame and Gray (2010), or the study by Crooks and Gray (2005) to avoid contamination of the QBO regressors by the solar signal or other regressors[ales](r4,sc6). The three principal components explain 49%, 47% and 3% of the total variance for the MERRA; 60%, 38% and 2% for the JRA-55; 59%, 37% and 3% for the ERA-Interim[ales](r4,sc6). The extraction of the first two components reveals a 28 month periodicity and an out-of phase relationship between the upper and lower stratosphere. The out-of phase relationship or orthogonality manifests approximately in a quarter period shift of these components. The deviation from the QBO quasi-regular period represented by the first two dominant components is contained in the residual variance of 4%[ales]. Linear regression analysis of the zonal wind with the inclusion of the first two principal components reveals a statistically significant linkage between the third principal component and the residuals of this analysis. Furthermore, the regression coefficient of this QBO proxy was statistically significant for all variables ~~tested for a~~[ales] p-value < 0.05 (see below for details about significance testing~~statistical significance~~[ales] techniques). Wavelet analysis for the MERRA[ales] demonstrates three statistically significant but non-stationary periods exceeding the level of the white noise wavelet spectrum (not shown): an approximate annual cycle (a peak period of 1 year and 2 months), a cycle with a peak period of 3 years and 3 months and a long-period cycle (a peak period between 10 and 15 years). Those interferences can be attributed to the possible non-linear interactions between the QBO itself and other signals like the annual cycle or long-period cycle such as the 11-year solar cycle at the equatorial stratosphere.

The El Niño Southern Oscillation (ENSO) is represented by the Multivariate ENSO index (MEI) which is computed as the first principal component of the six main observed variables over the Pacific Ocean: sea level pressure, zonal and meridional wind, sea surface temperature, surface air temperature and total cloudiness fraction of the sky (NCAR, 2013). The effect of volcanic eruptions is represented by the Stratospheric Aerosol Optical Depth

(SAOD). The time series was derived from the optical extinction data (Sato et al., 1993). We have used globally averaged time series in our regression model. The North Atlantic Oscillation (NAO) has also been included through itsin the respective[ales] index derived by a[ales] rotated principal component analysis technique[ales] applied to the monthly standardized 500-hPa height anomalies obtained from the Climate Data Assimilation System (CDAS) in the Atlantic region between 20°N-90°N (NOAA, 2013).

The robustness of solar regression coefficient has been tested in terms of including or excluding particular regressors in the regression model, e.g. NAO term was removed from the model and resulting solar regression coefficient was compared with the solar regression coefficient from the original regression setup. The solar regression coefficient seems to be highly robust since neither the amplitude nor statistical significance field was not changed significantly when NAO or QBO_3 or both of them were removed. However, cross-correlation analysis reveals that the correlation between NAO and TREND, SOLAR and SAOD regressors is statistically significant, but small (not shown).[ales](r1,c3,c4;r3,c13;r4,sc7)

The multiple regression model via eq. (1) has been used for the attribution analysis, and supplemented by two nonlinear techniques. The MLR coefficients were estimated by the least squares method. To avoid the effect of autocorrelation of residuals and to obtain the Best Linear Unbiased Estimate (BLUE) according to the Gauss-Markov theorem (Thejll, 2005), we have used an iterative algorithm to model the residuals as a second-order autoregressive process. Durbin-Watson test confirmed that this setup was sufficient to model most of the residual autocorrelations in the data.we have used an iterative algorithm to model the residuals as a second-order autoregressive process. The Durbin-Watson statistic has been used to detect the autocorrelation of the error terms from the regression model.[ales](r2,sc15)

As a result of the uncorrelated residuals, we can suppose the standard deviations of the estimated regression coefficients not to be diminished (Neter et al., 2004). The statistical significance of the regression coefficients was computed with a t-test and verified by a bootstrap significance test.

The nonlinear approach, in our case, consisted of Multi Layer Perceptron (MLP) and the relatively novel epsilon[ales](r4,sc9) Support Vector Regression (ε–[ales](r4,sc9)SVR) tech-

nique with the threshold parameter $\varepsilon = 0.1$[ales](r4,sc9) ~~in our case~~[ales](r4,tc9). The MLP as a technique inspired by the human brain is~~highly complex and~~[ales](r4,sc8) capable of capturing non-linear interactions between inputs (regressors) and output (modelled data) (e.g. Haykin, 2009). The nonlinear approach is achieved by transferring the input signals through a sigmoid function in a particular neuron and within a hidden layer propagating to the output (a so called feed–[ales](r3,c16)forward propagation). The standard error back–[ales](r3,c16)propagation iterative algorithm to minimize the global error has been used.

The Support Vector Regression technique belongs to the category of kernel methods. Input variables were nonlinearly transformed to a high-dimensional space by a radial basis (Gaussian) kernel, where a linear classification (regression) can be constructed (Cortes and Vapnik, 1995). However, cross-validation must be used to establish a kernel parameter and cost function searched in the logarithmic grid from 10^{-5} to 10^{1} and from 10^{-2} to 10^{5} respectively[ales](r4,sc9). We have used 5-fold cross-validation to optimize the SVR model selection for every point in the dataset as a trade-off between the recommended number of folds (Kohavi et al., 1995) and computational time. The MLP model was validated by the holdout method since this method is more expensive in order of magnitude compared to computational time. The datasets were separated into a training set (75% of the whole dataset) and a testing set (25% of the whole dataset). The neural network model was restricted to only one hidden layer with the maximum number of neurons set up to 20.[ales](r4,sc9)

The earlier mentioned lack of explanatory power of the nonlinear techniques in terms of complicated interpretation of statistical models (Olden and Jackson, 2002)[ales](r4,sc10) mainly comes from nonlinear interactions during signal propagation and the impossibility to directly monitor the influence of the input variables. In contrast to the linear regression approach, the understanding of relationships between variables is quite problematic. For this reason, the responses of our variables have been modelled by a technique originating from sensitivity analysis studies and also used by e.g. Blume and Matthes (2012). The

relative impact RI of each variable was computed as

$$RI = \frac{I_k}{\sum I_k}, \tag{2}$$

where $I_k = \sigma(\hat{y} - \hat{y_k})$. $\sigma(\hat{y} - \hat{y_k})$ is variance of[ales](r4,sc12) difference between the original model output $\hat{y}$ and the model output $\hat{y_k}$ when the k-input variable was held at its constant level. There are many possibilities with regard to which constant level to choose. It is possible to choose several levels and then to observe the sensitivity of model outputs varying for example on minimum, median and maximum levels. Our sensitivity measure (relative impact) was based on the median level. The primary reason comes from purely[ales](r3,c17) practical considerations - to compute our results fast enough as another weakness of the nonlinear techniques lies in the larger requirement of computational capacity. In general, this approach was chosen because of their relative simplicity for comparing all techniques to each other and to be able to interpret them too. The contribution of variables in neural network models has already been studied and Gevrey et al. (2003) produced a review and comparison of these methods.

4 Results

4.1 Annual response (MERRA)

Figure 1(a,d,g,j) shows the annually averaged solar signal in the zonal and altitudinal means of temperature, zonal wind, geopotential height and ozone mixing ratio. The signal is expressed as the average difference between the solar maxima and minima in the period 1979-2013, i.e. normalized by 126.6 solar radio flux units[ales](r3,c14;r4,sc13). Statistically significant responses detected by the linear regression in the temperature series (see Fig. 1(a)) are positive and are located around the equator in the lower stratosphere with values of about 0.5K. The temperature response increases to 1K in the upper stratosphere at the equator and up to 2K at the poles. The significant solar signal anomalies are more

variable around the stratopause and not limited to the equatorial regions. Hemispheric asymmetry of the statistical significance can be observed in the lower mesosphere. From a relative impact point of view (in Figs. 2(a)-(c) marked as RI), it is difficult to detect a signal with an impact larger than 20% in the lower stratosphere where the volcanic and QBO impacts dominate. In the upper layers (where the solar signal expressed by the regression coefficient is continuous across the equator) we have detected relatively isolated signals (over 20%) around $\pm 15^{\circ}$ using the relative impact method. The hemispheric asymmetry also manifests in the relative impact field, especially in the SVR field in the mesosphere.

The annually averaged solar signal in the zonal-mean of zonal wind (Figs. 1(d) and 2(d)-(f)) dominates around the stratopause as an enhanced subtropical westerly jet. The zonal wind variability due to the solar cycle corresponds with the temperature variability due to the change of the meridional temperature gradient and via the thermal wind equation. The largest positive anomaly in the northern hemisphere reaches 4 m/s around 60 km (Fig. 1(d)). In the southern hemisphere, the anomaly is smaller and not statistically significant. There is a significant negative signal in the southern polar region and also at the equator especially in the mesosphere. The negative anomalies correspond with a weakening of the westerlies or an amplification of the easterlies. The relative impact of the solar cycle is similarly located zonally even for both nonlinear techniques (Figs. 2(d)-(f)). The equatorial region across all the stratospheric layers is dominantly influenced by the QBO (expressed by all 3 QBO regressors) and for this reason the solar impact is minimized around the equator.

The pattern of the solar response in geopotential height (Figs. 1(g) and 2(g)-(i)) shows positive values in the upper stratosphere and lower mesosphere. This is also consistent with the zonal wind field thorough thermal wind balance. In the geopotential field, the solar cycle influences the most extensive area among all regressors. The impact area includes almost the whole mesosphere and the upper stratosphere.

The ~~last row of~~ales figure 1(j) also shows the annual mean solar signal in the zonal mean of the ozone mixing ratio (expressed as a percent change from the solar maximum to the solar minimum). By including EESC regressor term in the regresssion model ~~Using the~~

~~model with EESC~~[ales](r2,sc17) instead of a linear trend over the whole period (for more detailed description see methodology section)[ales](r2,sc17), we tried to capture the ozone trend change around the year 1996. Another possibility was to use our model over two individual periods, e.g. 1979-1995 and 1996-2013, but the results were quantitatively similar. The main common feature of other results is the positive ozone response in the lower stratosphere, ranging from a 1 to 3 percent change. The majority of results share the positive ozone response. In the equatorial upper stratosphere, no other relevant solar signal was detected compared to the study based on satellite measurement (Soukharev and Hood, 2006). By the relative impact method (Figs. 2(j)-(l)), we have obtained results comparable with linear regression coefficients, but especially around the stratopause the impact suggested by nonlinear techniques does not reach the values achieved by linear regression.

4.1.1 Annual response — C(~~e~~[ales](t4,tc6)omparison with JRA-55, ERA-Interim~~)~~[ales](t4,tc7)

Comparison of the results for the MERRA, ERA-Interim and JRA-55 temperature, zonal wind and geopotential height shows that the annual responses to the solar signal are in qualitative agreement (compare Figs. in 1). The zonal wind and geopotential response seems to be consistent in all presented methods and datasets. The largest discrepancies can be seen in the upper stratosphere and especially in the temperature field (the first row in these figures). The upper stratospheric equatorial anomaly was not detected by any of the regression techniques in the case of the JRA-55 reanalysis although the JRA-25 showed a statistically significant signal with structure and amplitude of 1-1.25 K comparable with ERA-Interim in the equatorial stratopause Mitchell et al. (2014a)[ales](r2,sc16). Furthermore~~On the other hand~~[ales], the anomaly in the MERRA~~ERA-Interim~~[ales](r2,sc16) temperature in Fig. 1(a) almost reaches the same value as in the ERA-Interim~~MERRA~~[ales] series nevertheless the upper-stratospheric equatorial signal is situated lower down at around 3 hPa Mitchell et al. (2014a)[ales](r2,sc16). However, upper-stratospheric temperature response could be less than accurate due to the existence of discontinuities in 1979, 1985 and 1998 (McLandress et al., 2013) coinciding with solar maxima. Therefore, the temperature response to solar variation may be influenced by these discontinuities in the upper stratosphere. The revised

analysis with the adjustments from McLandress et al. (2013) showed in comparison with the original analysis without any adjustment that the most pronounced differences are apparent in higher latitudes and especially in 1 hPa. However, the regression coefficients decreased by about 50% when using adjusted dataset and the differences are not statistically significant in terms of 95% confidence interval. The difference in tropical latitudes is about 0.2 K/(Smax-Smin). The trend regressor t from Eq. 1 reveal large turnaround from positive trend to negative in the adjusted levels, i.e. 1, 2, 3 and 5 hPa. Other regressors do not reveal any remarkable difference. The results in Figs. 1(b,e,h,k) and 3 from raw dataset ware kept in order to refer and discuss the accordance and difference between our results and results from Frame and Gray (2010); Mitchell et al. (2014a), where no adjustment has not considered as well.[ales](r3,c2,c19)

The variability of the solar signal in the MERRA stratospheric ozone series was compared with the ERA-Interim results. The analysis points to large differences in the ozone response to the solar cycle between the reanalyses and even in comparison with satellite measurements by Soukharev and Hood (2006). In comparison with the satellite measurements, no relevant solar signal was detected in the upper stratosphere in the MERRA series. The signal seems to be shifted above the stratopause (confirmed by all techniques, shown in Figs. 2 and 3(j)-(l)). Regarding the ERA-Interim, there is an ozone response to the solar cycle in the upper stratosphere. This statistically significant response indicates negative anomalies with values reaching up to 2% above the equator and up to 5% in the polar regions of both hemispheres. The negative response could be interpreted as a consequence of temperature rise leading to increased ozone losses because of the temperature dependence of the reaction rates that control the ozone balance in the upper stratosphere. This interpretation does not require that the assimilation model had included interactive ozone chemistry since in the model used for ERA-Interim the ozone as a prognostic variable is relaxed towards a photochemical equilibrium for the local value of the ozone mixing ratio, the temperature, and the overhead ozone column (Dee et al., 2011). An additional term is used to parameterize the heterogeneous chemistry. This fact together with the finding that the temperature and ozone are highly negatively correlated in the upper stratosphere, e.g. -0.93 for zonal mean

between 15°S and 15°N in 1 hPa, provide reasonable explanation of the negative ozone response to the SC which is driven by temperature variability in the upper stratosphere. In the case of MERRA, while SBUV ozone profiles are assimilated with solar cycle passed to forecast model (as ozone analysis tendency contribution), no solar cycle was passed to the radiative part of the model. The same is also true for ERA-Interim and JRA-55 (see descriptive table of reanalysis product on SC in irradiance and ozone in Mitchell et al. (2014a). Among other tendencies the dynamics and chemistry components also contribute to total tendency of ozone. These two tendencies prevent any variations in ozone analysis tendency though. Thus periods longer than 1 year are filtered out in the upper stratosphere. Only annual and semi-annual cycles are included. The SC-like periods seem to be diminishing approximately from 5 hPa except in the polar regions fro both hemispheres. The negative correlation -0.93 between the tendency of dynamics and chemistry and tendency from analysis for zonal mean in the tropical upper stratosphere confirms this statement as well. This negative correlation roots from anti-phase relationship between the tendency from dynamics and chemistry. Therefore despite the fact that the analyzed ozone should contain a solar signal, the signal is very weak and is compensated by internal model variability in terms of dynamics and chemistry. Since the SBUV ozone profiles have very low vertical resolution this may also affect the ozone response to the SC in the reanalysis. These facts should be also taken into account in case of monthly response discussion of particular variables in the section 4.2.~~The negative response can be connected with a higher destruction of ozone during the solar maximum period and consequent heating of the region.~~[ales](r3,c1;r4,sc14) The lower stratospheric ozone response~~solar signal~~[ales](r4,sc15) in the ERA-interim is not limited to the equatorial belt $\pm 30^{\circ}$ up to 20 hPa, as in the case of the MERRA reanalysis, and the statistical significance of this signal is rather reduced. The solar signal is detected higher and extends from the subtropical areas to the polar regions. The results suggest that the solar response in the MERRA series is more similar to the results from satellite measurements (Soukharev and Hood, 2006). Nevertheless, further comparison with independent data sets is needed to assess the data quality in detail.

4.1.2 Comparison of the linear and nonlinear approaches (MLR vs. SVR & MLP)

In this paper, we have applied and compared one linear (MLR) and two nonlinear attribution (SVR and MLP) techniques. The response of the studied variables to the solar signal and other forcings was studied using the sensitivity analysis approach i[ales](r2,sc18)n terms of averaged response deviation from the equilibrium represented by the original model output $\hat{y}$ (Blume and Matthes, 2012). This approach does not recognize a positive or negative response as the linear regression does. For this reason, the relative impact results are compared to the regression's coefficients. Using linear regression, it would be possible to assessanalyse[ales](r2,sc18) the statistical significance of the regression's coefficients and a particular level of the relative impact since they are linearly proportional[ales](r2,sc18). ~~Due to a higher variance, the significance levels of the relative impact are not estimated.~~[ales](r2,sc18) A comparison between the linear and nonlinear approaches by the relative impact fields shows qualitative and in most regions also quantitative agreement. The most pronounced agreement is observed in the zonal wind (Figs. 2, 3 and 4(d)-(f)) and geopotential height fields (Figs. 2, 3 and 4(g)-(i)). On the other hand the worst agreement is captured in the ozone field where nonlinear techniques have a problem identifying the upper stratospheric ozone anomaly detected by linear regression, although the lower stratospheric ozone anomaly is represented similarly by all techniques. In the temperature field the upper stratospheric solar signal reaches values over 20%, some individual signals in the Southern Hnorthern h[ales](r4,sc16)emisphere even reach 40%. However, using the relative impact approach, the lower stratospheric solar signal in the temperature field (which is well established by the regression coefficient) does not even reach 20% because of the dominance the QBO and volcanic effects. These facts emphasize that nonlinear techniques contribute to the robustness of attribution analysis since the linear regression results were plausibly confirmed by the SVR and MLP techniques.

In conclusion t~~However, the statistical significance of individual responses could have been estimated by the bootstrap technique, which is quite expensive for computational time, and for this reason was not applied. T~~[ales](r4,sc18)he comparison of various statis-

tical approaches (MLR, SVR and MLP) should actually contribute to the robustness of the attribution analysis including the statistically assessed uncertainties. These uncertainties could partially stem from the fact that the SVR and Neural network techniques are dependent on an optimal model setting which is based on a rigorous cross-validation process, which places a high demand on computing time.

The major differences between the techniques can be seen in how much of the temporal variability of the original time series is explained~~they can simulate the original time series~~[ales](r4,sc19), i.e. in the coefficient of determination. For instance, the differences of the explained variance reach up to 10% between linear and nonlinear techniques, although the zonal[ales] structure of the coefficient of determination is almost the same. To conclude, nonlinear techniques show an ability to simulate the middle atmosphere variability with a higher accuracy than cross-validated linear regression.

4.2 Monthly response (MERRA)

As was pointed out by Frame and Gray (2010), it is necessary to examine the solar signal in individual months because of a solar impact on polar-night jet oscillation Kuroda and Kodera (2001)~~variable solar impact throughout the year~~[ales](r2,sc20). For example, the amplitude of the lower stratospheric solar signal in the northern polar latitudes in February exceeds the annual response since the solar cycle influence on vortex stability is most pronounced in February. Besides the radiative influences of the solar cycle, we discuss the dynamical response throughout the polar winter (Kodera and Kuroda, 2002).

Statistically significant upper stratospheric equatorial anomalies in the temperature series (winter months in Figs. 5 and 6(a)-(d)) are expressed in almost all months. Their amplitude and statistical significance vary throughout the year. The variation between the solar maxima and minima could be up to 1K in some months. Outside the equatorial regions, the fluctuation could reach several kelvins. The lower stratospheric equatorial anomaly strengthens during winter. This could be an indication of dynamical changes, i.e. alteration~~alternation~~[ales](r4,tc9) of the residual circulation between the equator and polar regions (for details please see section 5)~~the discussion~~[ales]. Aside from the radiative forcing

by direct or ozone heating, other factors are linked to the anomalies in the upper levels of the middle atmosphere (Haigh, 1994; Gray et al., 2009). It is necessary to take into consideration the dynamical coupling with the mesosphere through changes of the residual circulation (see the ~~below~~[ales] dynamical effects discussion below[ales]). That can be illustrated by the positive anomaly around the stratopause in February (up to 4K around 0.5 hPa). This anomaly extends further down~~propagates downward~~[ales](r4,sc20) and, together with spring radiative forcing, affects the stability of the equatorial stratopause. Hemispheric asymmetry in the temperature response above the stratopause probably originates from the hemispheric differences, i.e. different wave activity (Kuroda and Kodera, 2001)[ales](r2,sc21). These statistically significant and positive temperature anomalies across the subtropical stratopause begin to descend and move to higher latitudes in the beginning of the northern winter. The anomalies manifest fully in February in the region between $60^\circ - 90^\circ$N and ~~below 10 hPa and~~[ales](r4,sc21) reach tropospheric levels - contrary to the results for the southern hemisphere(see Fig. 10 in Mitchell et al., 2014a)[ales](r4,sc21). The southern hemispheric temperature anomaly is persistent above the stratopause and the solar cycle influence on the vortex stability differs from those in the northern hemisphere.

The above described monthly anomalies of temperature correspond with the zonal wind anomalies throughout the year (Figs. 5 and 6(e)-(h)). The strengthening of the subtropical jets around the stratopause is most apparent during the winter in both hemispheres. This positive zonal wind anomaly gradually descends and moves poleward similar to Frame and Gray (2010) analysis based on ERA-40 data. In February, the intensive stratospheric warming and mesospheric cooling is associated with a more pronounced transition from winter to summer circulation attributed to the solar cycle (in relative impact methodology up to 30%). However, GCMs have not yet successfully simulated the strong warming in February (e.g. Schmidt et al., 2010; Mitchell et al., 2015). Due to the short (35-year) time series, it is possible that this pattern is not really solar in origin but is instead a consequence of internal climate variability or aliasing from effects of the two major volcanic eruptions aligned to solar maximum periods Chiodo et al. (2014).[ales](r3,c4)

In the southern hemisphere, this poleward motion of the positive zonal wind anomaly halts approximately at 60°S. For example in August, we can observe a well-marked latitudinal zonal wind gradient (Fig. 5(g)). Positive anomalies in the geopotential height field correspond with the easterly zonal wind anomalies. The polar circulation reversal is associated with intrusion of ozone from the lower latitudes as it is apparent, e.g., in August in the southern hemisphere and in February in the northern hemisphere (last rows of Figs. 5 and 6).

When comparing the results fromof[ales] the MERRA and ERA-40 series studied by Frame and Gray (2010), distinct differences were found (Figs. 5(e)-(f)) in the equatorial region of the lower mesosphere in October and November. W~~, w~~[ales](r3,c20)hile in the MERRA reanalysis we have detected an easterly anomaly above 1 hPa in both months (only November shown)[ales](r4,sc23), a westerly anomaly was identified in the ERA-40 series. Further distinct differences in the zonal mean temperature and zonal wind anomalies were not found.

5 Dynamical effects discussion

In this section, we discuss the dynamical impact of the solar cycle and its influence on middle atmospheric winter conditions. Linear regression was applied to the EP diagnostics. Kodera and Kuroda (2002) suggested that the solar signal produced in the upper stratosphere region is transmitted to the lower stratosphere through the modulation of the internal mode of variation in the polar night jet and through a change in the Brewer-Dobson circulation (prominent in the equatorial region in the lower stratosphere). In our analysis, we discussed the evolution of the winter circulation with an emphasis on the vortex itself rather than the behavior of the jets. Further, we try to describededuce[ales](r3,c21) the possible processes leading to the observed differences in the quantities of state between the solar maximum and minimum period. Because the superposition principle only holds for linear processes, it is impossible to deduce the dynamics merely from the fields of differences. As noted by Kodera and Kuroda (2002), the dynamical response of the winter

stratosphere includes highly nonlinear processes, e.g. wave mean flow interactions. Thus, both the anomaly and the total fields, including climatology, must be taken into account.

We start the analysis of solar maximum dynamics with the period of the northern hemispheric winter circulation formation. The anomalies of the ozone, temperature, geopotential and Eliassen-Palm flux divergence support the hypothesis of weaker BDC during the solar maximum due to the less intensive wave pumping. This is consistent with previous studies (Kodera and Kuroda, 2002; Matthes et al., 2006). The causality is unclear, but the effect is visible in both branches of BDC as is illustrated~~explained~~[ales] by Fig. 5 and summarized schematically in Fig. 7.

During the early Northern hemispheric (NH) winter (including November)~~November~~[ales] (r2,sc2) when westerlies develop in the stratosphere, we can observe a deeper polar vortex and consequent stronger westerly winds both inside and outside the vortex. However, only the westerly anomaly outside the polar region and around 30°N from 10 hPa to the lower mesosphere is statistically significant (see the evolution of zonal wind anomalies in Figs. 5(e)-(h)). The slightly different wind field has a direct influence on the vertical propagation of planetary waves. From the Eliassen-Palm flux anomalies and climatology we can see that the waves propagate vertically with increasing poleward instead of equatorward meridional direction with height. This is then reflected in the EP flux divergence field, where the region of maximal convergence is shifted poleward and the anomalous convergence region emerges inside the vortex above approximately 50 hPa (Figs. 5(m)-(p)).

The poleward shift of the maximum convergence area further contributes to the reduced BDC. This is again confirmed by the temperature and ozone anomalies. The anomalous convergence inside the vortex induces anomalous residual circulation, the manifestation of which is clearly seen in the quadrupole-like temperature structure (positive and negative anomalies are depicted schematically in Fig. 7 using red and blue boxes respectively). This pattern emerges in November and even more clearly in December. In December, the induced residual circulation leads to an intrusion of the ozone rich air into the vortex at about the 1 hPa level (Fig. 5(s)). The inhomogeneity in the vertical structure of the vortex is then also pronounced in the geopotential height differences. This corresponds with the

temperature analysis in the sense that above and in the region of the colder anomaly there is a negative geopotential anomaly and vice versa. The geopotential height difference has a direct influence on the zonal wind field (via the thermal wind balance). The result is a deceleration of the upper vortex parts and consequent broadening of the upper parts (due to the conservation of angular momentum).

Considering the zonal wind field, the vortex enters January approximately with its average climatological extent. The wind speeds in its upper parts are slightly higher. This is because of the smaller geopotential values corresponding to the negative temperature anomalies above approximately 1 hPa. This probably[ales](r2,sc23) results from the absence of adiabatic heating due to the suppressed BDC, although the differences in the quantities of state (temperature and geopotential height) are small and insignificant (see the temperature anomalies in Fig. 5(c)). It is important to note that these differences change sign around an altitude of 40 km inside the vortex further accentuating the vertical inhomogeneity of the vortex. This might start balancing processes inside the vortex, which is confirmed by analysis of the dynamical quantities, i.e. EP flux and its divergence (Fig. 5(o)). ~~A detailed description of these processes is the key to understanding the dynamics and causality of Sudden Stratospheric Warmings (SSWs) taking place in February.~~[ales](r4,sc25)

Significant anomalies of the EP flux indicate anomalous vertical wave propagation resulting in the strong anomalous EP flux convergence being significantly pronounced in a horizontally broad region and confined to upper levels (convergence (negative values) drawn by green or blue shades in Figs. 5(m)-(p)). This leads to the induction of an anomalous residual circulation starting to gain intensity in January. The situation then results in the disruption of the polar vortex visible in significant anomalies in the quantities of state in February – in contrast to January. Further strong mixing of air is suggested by the ozone fields. The quadrupole-like structure of the temperature is visible across the whole NH middle atmosphere in February (indicated in the lower diagram of Fig. 7), especially in the higher latitudes. This is very significant and well pronounced by the stratospheric warming and mesospheric cooling.

The hemispheric asymmetry of the solar cycle influence can be especially documented in winter conditions as was already suggested in section 4.2. Since the positive zonal wind anomaly halts at approximately 60°S and intensifies over 10 m/s, one would expect the poleward deflection of the planetary wave propagation to be according to NH winter mechanisms discussed above. This is actually observed from June to August when the highest negative anomalies of the latitudinal componentcoordinates[ales](r4,sc26) of EP flux are located in the upper stratosphere and in the lower mesosphere (Figs. 6(m)-(p)). The anomalous divergence of EP flux develops around the stratopause between 30°S and 60°S. Like the hypothetical mechanism of weaker BDC described above, we can observeassume[ales](r3,c22) less wave pumping in the stratosphere and consequently assume[ales](r3,c22) less upwelling in the equatorial region. In line with that, we can see in the lower stratosphere of equatorial region (Fig. 5(b) and 6(b)) a more pronounced temperature response in August (above 1 K) than in December (around 0.5 K) as already mentioned in previous observational (van Loon and Labitzke, 2000) or reanalysis (Mitchell et al., 2014a) studies. Although this can point to a more weakened BDC, the residual circulation (Fig. 6(q)-(t)) as a proxy for BDC (Butchart, 2014) does not reveal this signature. Hypothetically this could be due higher role of unresolved wave processes in reanalysis (small scale GW) or due to the worse performance of residual circulation as a proxy for the large-scale transport in SH (e.g. larger departure from steady waves approximation comparing to NH), or because of the other processes than BDC leading to the temperature anomaly, e.g. aliasing with volcanic signal.~~However, the anomalies of the residual circulation pointing to a weaker BDC are not so well established as in the case of the NH winter. These mechanisms could lead to an explanation for the more pronounced temperature response to the solar signal in the equatorial region of the lower stratosphere in August for the SH winter (above 1 K) than in December for the NH winter (around 0.5 K). This is in agreement with another observational study (van Loon and Labitzke, 200~~

Overall, the lower stratospheric temperature anomaly is more coherent for the SH winter than for the NH winter, where the solar signal is not so well apparent or statistically significant in particular months and reanalysis datasets.

6 Conclusions

We have analysed the changes of air temperature, ozone and circulation characteristics driven by the variability of the 11-year solar cycle's influence on the stratosphere and lower mesosphere. Attribution analysis was performed on the three reanalysed datasets: MERRA, ERA-Interim and JRA-55;~~last generation of reanalysed data,~~[ales](r4,sc27) and aimed to compare how these types of datasets resolve the solar variability throughout the levels where the "top-down" mechanism is assumed. Furthermore, the results originated in linear attribution using MLR were compared with other relevant attribution~~observational~~[ales](r4,sc29) studies and supported by nonlinear attribution analysis using SVR and MLP techniques.

The nonlinear approach to attribution analysis, represented by the application of the SVR and MLP, largely confirmed the solar response computed by linear regression. Consequently, these results can be considered quite robust regarding the statistical modeling of the solar variability in the middle atmosphere. This finding indicates that linear regression is a sufficient technique to resolve the basic shape of the solar signal through the middle atmosphere. However, some uncertainties could partially stem from the fact that the SVR and MLP techniques are highly dependent on an optimal model setting that requires a rigorous cross-validation process (which places a high demand on computing time). As a benefit, nonlinear techniques show an ability to[ales](r3,c25) simulate the middle atmosphere variability with higher accuracy than linear regression.

The solar signal extracted from the temperature field from MERRA and ERA-Interim reanalysis using linear regression has the amplitudes around 1K and 0.5K, in the upper stratospheric and in the lower stratospheric equatorial region, respectively. These signals, statistically significant at a p-value < 0.01, ~~can be considered sufficiently robust and they~~[ales](r4,sc28) are in qualitative agreement with previous attribution~~observational~~[ales](r4,sc29) studies (e.g. Frame and Gray, 2010; Mitchell et al., 2014a). ~~since we have used the generation of reanalysed datasets extended to 2013.~~[ales](r2,sc12) The statistically significant signal was only observed in the lower part of the stratosphere in the JRA-55 reanalysis, however with similar amplitudes as the other datasets.

Similar to the temperature response, the double-peaked solar response in ozone was detected in satellite measurements (e.g. Soukharev and Hood, 2006) and in spite of that the concerns about physical mechanism of the lower stratospheric response was expressed (e.g. Austin et al., 2008).~~even confirmed by the coupled chemistry climate model simulations (e.g. Austin et al., 2008).~~[ales](r3,c24) However, the exact position and amplitude of both ozone anomalies remain a point of disagreement between models and observations. The results of our attribution analysis point to large differences in the upper stratospheric ozone response to the solar cycle in comparison with the studies mentioned above and even between reanalyses themselves. The upper stratospheric ozone anomaly reaches 2% in the SBUV(/2) satellite measurements (e.g. Soukharev and Hood, 2006, Fig. 5) which were assimilated as the only source of ozone profiles in MERRA reanalysis. This fact is remarkable since the same signal was not detected in the upper stratosphere in the MERRA results. However, the solar signal in the ozone field seems to be shifted above the stratopause where similar and statistically significant solar variability was attributed. Concerning the solar signal in the ERA-Interim, there is a negative ozone response via a regression coefficient in the upper stratosphere although the solar variability expressed as relative impact appears to be in agreement with satellite measurements. Furthermore, the lower stratospheric solar response in the ERA-Interim's ozone around the equator is reduced in this dataset and shifted to higher latitudes. Another difference was detected in the monthly response of the zonal wind in October and November in the equatorial region of the lower mesosphere between the results for the MERRA series and ERA-40 data studied by Frame and Gray (2010). While in the MERRA reanalysis we have detected an easterly anomaly, a westerly anomaly was identified in the ERA-40 series.

A similar problem with the correct resolving of the double-peaked ozone anomaly was registered in the study of Dhomse et al. (2011) which investigated thein[ales](r3,c25) solar response in the tropical stratospheric ozone using a 3D chemical transport model. The upper stratospheric solar signal observed in SBUV/SAGE and SAGE-based data could only be reproduced in model runs with unrealistic dynamics, i.e. with no inter-annual meteorological changes.

The reanalyses have proven to be extremely valuable scientific tools (Rienecker et al., 2011). On the other hand, they have to be used with a caution for example, due the existence of large discontinuities occurring in 1979, 1985 and 1998 (McLandress et al., 2013) that translated into errors in the derived solar coefficients. For instance the revised analysis with the adjustments from McLandress et al. (2013) resulted to 0.2 K/(Smax-Smin) difference between regression coefficients in tropical latitudes of the upper stratosphere.[ales](r3,c23)

In the dynamical effects discussion, we described the dynamical impact of the solar cycle on middle atmospheric winter conditions. ~~The main part deals with the solar influence on northern winter conditions nevertheless, southern winter anomalies were also discussed.~~[ales](r3,c2
The relevant dynamical effects are summarized in schematic diagrams (Fig. 7). Both diagrams depict average conditions and anomalies induced by the solar cycle. The first one summarizes how equatorward wave propagation is influenced by the westerly anomaly around the subtropical stratopause. The quadrupole-like temperature structure is explained by anomalous residual circulation in the higher latitudes together with the anomalous branch heading towards the equatorial region already hypothesized by Kodera and Kuroda (2002). The second diagram concludes the transition time to vortex disruption during February. Again, a very apparent quadrupole-like temperature structure is even more pronounced, especially in the polar region and seems to be more extended to lower latitudes.

Fields of residual circulation and EP flux divergence in February are showing an opposite to what would be expected from the suppressed BDC in the SC max. There is an enhanced downwelling in polar and enhanced upwelling in eq. region under 1 hPa, suggesting the need to diagnose the influence of SC on transport at least on monthly scale because the changes in the underlying dynamics (compare upper and lower diagram in Fig. 7) would make the transport pathways more complicated.[ales](r1,c6) Since GCMs have not yet successfully simulated this pattern (e.g. Schmidt et al., 2010; Mitchell et al., 2015) and due to the short (35-year) time series, it is possible that this pattern is not really solar in origin but is instead a consequence of internal climate variability or aliasing from effects of the two major volcanic eruptions aligned to solar maximum periods (Chiodo et al., 2014).[ales](r1,c6;r3,c4)

However, we can strongly assume that the dynamical effects are not zonally uniform, as it is shownsupposed and presented[ales] here using two-dimensional (2D) EP diagnostics and TEM equations. Hence, it would be interestingSo it would be desirable[ales](r4,sc31) to extend the discussion of dynamical effects for other relevant characteristics, for example, for the analysis of wave propagation and wave-mean flow interaction using the 3D formulation (Kinoshita and Sato, 2013).

This paper is fully focused on the solar cycle influence, i.e. on decadal changes in the stratosphere and lower mesosphere, although a huge amount of results concerning other forcings was generated by attribution analysis. SThe QBO phenomenon could be one of them s[ales]ince the solar-QBO interaction and the modulation of Holton-Tan relationship by the solar cycle are regarded as highly challenging, especially in global climate simulations (Matthes et al., 2013).

Acknowledgements. The authors would like to thank to the relevant working teams for the reanalysis datasets: MERRA (obtained from NASA, http://disc.sci.gsfc.nasa.gov/daac-bin/DataHoldings.pl), ERA-Interim (obtained from ECMWF, http://apps.ecmwf.int/datasets/) and JRA-55 (obtained from http://jra.kishou.go.jp/JRA-55/index_en.html). Furthermore, we need to acknowledge python open-source software libraries used for this paper: MLR (Seabold and Perktold, 2010), SVR (Pedregosa et al., 2011) and MLP (Nissen, 2015).[ales](r4,sc9) We would also like to express our gratitude to C. A. Svoboda (Foreign Language Studies, Faculty of Mathematics and Physics, Charles University in Prague) for the proofreading of[ales] our paper. The study was supported by the Charles University in Prague, Grant Agency project No. 1474314, and by the grant No. SVV-2014-26096.

References

Andrews, D. G. and McIntyre, M. E.: JR Holton, and CB Leovy, 1987: Middle Atmosphere Dynamics, 1987.

Austin, J., Tourpali, K., Rozanov, E., Akiyoshi, H., Bekki, S., Bodeker, G., Brühl, C., Butchart, N., Chipperfield, M., Deushi, M., Fomichev, V. I., Giorgetta, M. A., Gray, L., Kodera, K., Lott, F., Manzini, E., Marsh, D., Matthes, K., Nagashima, T., Shibata, K., Stolarski, R. S., Struthers, H., and Tian, W.: Coupled chemistry climate model simulations of the solar cycle in ozone

and temperature, Journal of Geophysical Research, 113, D11 306, doi:10.1029/2007JD009391, http://doi.wiley.com/10.1029/2007JD009391, 2008.

Ball, W. T., Krivova, N. A., Unruh, Y. C., Haigh, J. D., and Solanki, S. K.: A new SATIRE-S spectral solar irradiance reconstruction for solar cycles 21–23 and its implications for stratospheric ozone, arXiv preprint arXiv:1408.0365, 2014.

Blume, C. and Matthes, K.: Understanding and forecasting polar stratospheric variability with statistical models, Atmos. Chem. Phys, 12, 5691–5701, 2012.

Butchart, N.: The Brewer-Dobson circulation, Reviews of Geophysics, 52, 157–184, doi:10.1002/2013RG000448, http://doi.wiley.com/10.1002/2013RG000448, 2014.

Camp, C. D. and Tung, K.: The influence of the solar cycle and QBO on the late-winter stratospheric polar vortex, Journal of the atmospheric sciences, 64, 1267–1283, 2007.

Chiodo, G., Calvo, N., Marsh, D., and Garcia-Herrera, R.: The 11 year solar cycle signal in transient simulations from the Whole Atmosphere Community Climate Model, Journal of Geophysical Research: Atmospheres (1984–2012), 117, 2012.

Chiodo, G., Marsh, D., Garcia-Herrera, R., Calvo, N., and García, J.: On the detection of the solar signal in the tropical stratosphere, Atmospheric Chemistry and Physics, 14, 5251–5269, 2014.

Cortes, C. and Vapnik, V.: Support-vector networks, Machine Learning, 20, 273–297, doi:10.1007/BF00994018, http://link.springer.com/10.1007/BF00994018, 1995.

Coughlin, K. and Tung, K.-K.: Eleven-year solar cycle signal throughout the lower atmosphere, Journal of Geophysical Research: Atmospheres (1984–2012), 109, 2004.

Crooks, S. A. and Gray, L. J.: Characterization of the 11-year solar signal using a multiple regression analysis of the ERA-40 dataset, Journal of climate, 18, 996–1015, 2005.

Dee, D., Uppala, S., Simmons, A., Berrisford, P., Poli, P., Kobayashi, S., Andrae, U., Balmaseda, M., Balsamo, G., Bauer, P., et al.: The ERA-Interim reanalysis: Configuration and performance of the data assimilation system, Quarterly Journal of the Royal Meteorological Society, 137, 553–597, 2011.

Dhomse, S., Chipperfield, M. P., Feng, W., and Haigh, J. D.: Solar response in tropical stratospheric ozone: a 3-D chemical transport model study using ERA reanalyses, Atmospheric Chemistry and Physics, 11, 12 773–12 786, doi:10.5194/acp-11-12773-2011, http://www.atmos-chem-phys.net/11/12773/2011/, 2011.

Ebita, A., Kobayashi, S., Ota, Y., Moriya, M., Kumabe, R., Onogi, K., Harada, Y., Yasui, S., Miyaoka, K., Takahashi, K., et al.: The Japanese 55-year Reanalysis (JRA-55): an interim report, Sola, 7, 149–152, 2011.

Edmon Jr, H., Hoskins, B., and McIntyre, M.: Eliassen-Palm cross sections for the troposphere, Journal of the Atmospheric Sciences, 37, 2600–2616, 1980.

Ermolli, I., Matthes, K., Dudok de Wit, T., Krivova, N. A., Tourpali, K., Weber, M., Unruh, Y. C., Gray, L., Langematz, U., Pilewskie, P., Rozanov, E., Schmutz, W., Shapiro, A., Solanki, S. K., and Woods, T. N.: Recent variability of the solar spectral irradiance and its impact on climate modelling, Atmospheric Chemistry and Physics, 13, 3945–3977, doi:10.5194/acp-13-3945-2013, http://www.atmos-chem-phys.net/13/3945/2013/, 2013.

Frame, T. H. A. and Gray, L. J.: The 11-Yr Solar Cycle in ERA-40 Data: An Update to 2008, Journal of Climate, 2010.

Fujiwara, M., Polavarapu, S., and Jackson, D.: A proposal of the SPARC reanalysis/analysis intercomparison project, SPARC Newsletter, 38, 14–17, 2012.

Gevrey, M., Dimopoulos, I., and Lek, S.: Review and comparison of methods to study the contribution of variables in artificial neural network models, Ecological Modelling, 160, 249–264, 2003.

Gray, L. J., Crooks, S., Pascoe, C., Sparrow, S., and Palmer, M.: Solar and QBO influences on the timing of stratospheric sudden warmings, Journal of the atmospheric sciences, 61, 2777–2796, 2004.

Gray, L. J., Rumbold, S., and Shine, K. P.: Stratospheric temperature and radiative forcing response to 11-year solar cycle changes in irradiance and ozone, Journal of the Atmospheric Sciences, 66, 2402–2417, 2009.

Gray, L. J., Beer, J., Geller, M., Haigh, J. D., Lockwood, M., Matthes, K., Cubasch, U., Fleitmann, D., Harrison, G., Hood, L., et al.: Solar influences on climate, Reviews of Geophysics, 48, RG4001, 2010.

Gray, L. J., Scaife, A. A., Mitchell, D. M., Osprey, S., Ineson, S., Hardiman, S., Butchart, N., Knight, J., Sutton, R., and Kodera, K.: A lagged response to the 11 year solar cycle in observed winter Atlantic/European weather patterns, Journal of Geophysical Research: Atmospheres, 118, 13,405–13,420, doi:10.1002/2013JD020062, http://dx.doi.org/10.1002/2013JD020062, 2013.

Haigh, J. D.: The role of stratospheric ozone in modulating the solar radiative forcing of climate, Nature, 370, 544–546, 1994.

Harder, J. W., Fontenla, J. M., Pilewskie, P., Richard, E. C., and Woods, T. N.: Trends in solar spectral irradiance variability in the visible and infrared, Geophysical Research Letters, 36, 2009.

Haykin, S. S.: Neural networks and learning machines, vol. 3, Pearson Education Upper Saddle River, 2009.

Holton, J. R. and Tan, H.-C.: The influence of the equatorial quasi-biennial oscillation on the global circulation at 50 mb, Journal of the Atmospheric Sciences, 37, 2200–2208, 1980.

Hood, L., Schimanke, S., Spangehl, T., Bal, S., and Cubasch, U.: The Surface Climate Response to 11-Yr Solar Forcing during Northern Winter: Observational Analyses and Comparisons with GCM Simulations, Journal of Climate, 26, 7489–7506, doi:10.1175/JCLI-D-12-00843.1, http://dx.doi.org/10.1175/JCLI-D-12-00843.1, 2013.

Hood, L. L. and Soukharev, B. E.: The Lower-Stratospheric Response to 11-Yr Solar Forcing: Coupling to the Troposphere-Ocean Response, Journal of the Atmospheric Sciences, 69, 1841–1864, doi:10.1175/JAS-D-11-086.1, http://dx.doi.org/10.1175/JAS-D-11-086.1, 2012.

Hood, L. L., Soukharev, B. E., and McCormack, J. P.: Decadal variability of the tropical stratosphere: Secondary influence of the El Niño–Southern Oscillation, Journal of Geophysical Research, 115, D11 113, 2010.

Ineson, S., Scaife, A. A., Knight, J. R., Manners, J. C., Dunstone, N. J., Gray, L. J., and Haigh, J. D.: Solar forcing of winter climate variability in the Northern Hemisphere, Nature Geoscience, 4, 753–757, 2011.

Kinoshita, T. and Sato, K.: A formulation of unified three-dimensional wave activity flux of inertia–gravity waves and Rossby waves, Journal of the Atmospheric Sciences, 70, 1603–1615, 2013.

Kodera, K. and Kuroda, Y.: Dynamical response to the solar cycle, Journal of Geophysical Research: Atmospheres, 107, ACL 5–1–ACL 5–12, doi:10.1029/2002JD002224, http://dx.doi.org/10.1029/2002JD002224, 2002.

Kohavi, R. et al.: A study of cross-validation and bootstrap for accuracy estimation and model selection, in: IJCAI, vol. 14, pp. 1137–1145, 1995.

Kren, A., Marsh, D., Smith, A., and Pilewskie, P.: Examining the stratospheric response to the solar cycle in a coupled WACCM simulation with an internally generated QBO, Atmospheric Chemistry and Physics, 14, 4843–4856, 2014.

Kuchar, A.: EPFD: Second release of EPFD python script, doi:10.5281/zenodo.16339, http://dx.doi.org/10.5281/zenodo.16339, 2015.

Kuroda, Y. and Kodera, K.: Variability of the polar night jet in the Northern and Southern Hemispheres, Journal of Geophysical Research: Atmospheres (1984–2012), 106, 20 703–20 713, 2001.

Labitzke, K.: Sunspots, the QBO, and the stratospheric temperature in the north polar region, Geophysical Research Letters, 14, 535–537, doi:10.1029/GL014i005p00535, http://dx.doi.org/10.1029/GL014i005p00535, 1987.

Labitzke, K., Kunze, M., and Bronnimann, S.: Sunspots, the QBO and the stratosphere in the North Polar Region 20 years later, Meteorologische Zeitschrift, 15, 355–363, 2006.

Lean, J.: Short term, direct indices of solar variability, Solar Variability and Climate, pp. 39–51, 2001.

Lee, H. and Smith, A. K.: Simulation of the combined effects of solar cycle, quasi-biennial oscillation, and volcanic forcing on stratospheric ozone changes in recent decades, Journal of Geophysical Research: Atmospheres, 108, n/a–n/a, doi:10.1029/2001JD001503, http://dx.doi.org/10.1029/2001JD001503, 2003.

Matthes, K., Langematz, U., Gray, L. L., Kodera, K., and Labitzke, K.: Improved 11-year solar signal in the Freie Universität Berlin climate middle atmosphere model (FUB-CMAM), Journal of Geophysical Research: Atmospheres (1984–2012), 109, 2004.

Matthes, K., Kuroda, Y., Kodera, K., and Langematz, U.: Transfer of the solar signal from the stratosphere to the troposphere: Northern winter, Journal of geophysical research, 111, D06 108, 2006.

Matthes, K., Marsh, D. R., Garcia, R. R., Kinnison, D. E., Sassi, F., and Walters, S.: Role of the QBO in modulating the influence of the 11 year solar cycle on the atmosphere using constant forcings, Journal of Geophysical Research: Atmospheres (1984–2012), 115, 2010.

Matthes, K., Kodera, K., Garcia, R. R., Kuroda, Y., Marsh, D. R., and Labitzke, K.: The importance of time-varying forcing for QBO modulation of the atmospheric 11 year solar cycle signal, Journal of Geophysical Research: Atmospheres, 118, 4435–4447, doi:10.1002/jgrd.50424, http://doi.wiley.com/10.1002/jgrd.50424, 2013.

McLandress, C., Plummer, D., and Shepherd, T.: Technical Note: A simple procedure for removing temporal discontinuities in ERA-Interim upper stratospheric temperatures for use in nudged chemistry-climate model simulations, Atmospheric Chemistry and Physics Discussions, 13, 25 801–25 825, 2013.

Mitchell, D., Gray, L., Fujiwara, M., Hibino, T., Anstey, J., Ebisuzaki, W., Harada, Y., Long, C., Misios, S., Stott, P., et al.: Signatures of naturally induced variability in the atmosphere using multiple reanalysis datasets, Quarterly Journal of the Royal Meteorological Society, 2014a.

Mitchell, D., Montabone, L., Thomson, S., and Read, P.: Polar vortices on Earth and Mars: A comparative study of the climatology and variability from reanalyses, Quarterly Journal of the Royal Meteorological Society, 2014b.

Mitchell, D. M., Misios, S., Gray, L. J., Tourpali, K., Matthes, K., Hood, L., Schmidt, H., Chiodo, G., Thiéblemont, R., Rozanov, E., Shindell, D., and Krivolutsky, A.: Solar Signals in CMIP-5 Simulations: The Stratospheric Pathway, Quarterly Journal of the Royal Meteorological Society, pp. n/a–n/a, doi:10.1002/qj.2530, http://doi.wiley.com/10.1002/qj.2530, 2015.

NCAR: The Climate Data Guide: Multivariate ENSO Index, Retrieved from https://climatedataguide.ucar.edu/climate-data/multivariate-enso-index, last modified 20 Aug 2013, 2013.

Neter, J., Kutner, M., Wasserman, W., and Nachtsheim, C.: Applied Linear Statistical Models, McGraw-Hill/Irwin, 2004.

Nissen, S.: Fast Artificial Neural Network Library (FANN), https://github.com/libfann/fann, 2015.

NOAA: Northern Atlantic Oscillation index, Retrieved from http://www.cpc.ncep.noaa.gov/products/precip/CWlink/pna/nao.shtml, last modified daily, 2013.

Olden, J. D. and Jackson, D. A.: Illuminating the "black box": a randomization approach for understanding variable contributions in artificial neural networks, Ecological Modelling, 154, 135–150, doi:10.1016/S0304-3800(02)00064-9, http://linkinghub.elsevier.com/retrieve/pii/S0304380002000649, 2002.

Pasini, A., Lorè, M., and Ameli, F.: Neural network modelling for the analysis of forcings/temperatures relationships at different scales in the climate system, Ecological Modelling, 191, 58–67, doi:10.1016/j.ecolmodel.2005.08.012, http://linkinghub.elsevier.com/retrieve/pii/S0304380005003492, 2006.

Pedregosa, F., Varoquaux, G., Gramfort, A., Michel, V., Thirion, B., Grisel, O., Blondel, M., Prettenhofer, P., Weiss, R., Dubourg, V., Vanderplas, J., Passos, A., Cournapeau, D., Brucher, M., Perrot, M., and Duchesnay, E.: Scikit-learn: Machine Learning in Python, Journal of Machine Learning Research, 12, 2825–2830, 2011.

Pisoft, P., Holtanova, E., Huszar, P., Miksovsky, J., and Zak, M.: Imprint of the 11-year solar cycle in reanalyzed and radiosonde datasets: a spatial frequency analysis approach, Climatic Change, 110, 85–99, doi:10.1007/s10584-011-0147-0, http://dx.doi.org/10.1007/s10584-011-0147-0, 2012.

Pisoft, P., Holtanova, E., Huszar, P., Kalvova, J., Miksovsky, J., Raidl, A., Zemankova, K., and Zak, M.: Manifestation of reanalyzed QBO and SSC signals, Theoretical and Applied Climatology, pp. 1–10, 2013.

Randel, W. J. and Wu, F.: A stratospheric ozone profile data set for 1979–2005: Variability, trends, and comparisons with column ozone data, Journal of Geophysical Research: Atmospheres (1984–2012), 112, 2007.

Rienecker, M. M., Suarez, M. J., Gelaro, R., Todling, R., Bacmeister, J., Liu, E., Bosilovich, M. G., Schubert, S. D., Takacs, L., Kim, G. K., et al.: MERRA: NASA's modern-era retrospective analysis for research and applications, Journal of Climate, 24, 3624–3648, 2011.

Sato, M., Hansen, J. E., McCormick, M. P., and Pollack, J. B.: Stratospheric aerosol optical depths, 1850-1990, Journal of Geophysical Research: Atmospheres, 98, 22 987–22 994, doi:10.1029/93JD02553, http://dx.doi.org/10.1029/93JD02553, 1993.

Scaife, A. A., Ineson, S., Knight, J. R., Gray, L., Kodera, K., and Smith, D. M.: A mechanism for lagged North Atlantic climate response to solar variability, Geophysical Research Letters, 40, 434–439, 2013.

Schmidt, H., Brasseur, G. P., and Giorgetta, M. A.: Solar cycle signal in a general circulation and chemistry model with internally generated quasi-biennial oscillatio, Journal of Geophysical Research: Atmospheres, 115, doi:10.1029/2009JD012542, 2010.

Seabold, S. and Perktold, J.: Statsmodels: Econometric and statistical modeling with python, in: Proceedings of the 9th Python in Science Conference, 2010.

Seviour, W. J., Butchart, N., and Hardiman, S. C.: The Brewer–Dobson circulation inferred from ERA-Interim, Quarterly Journal of the Royal Meteorological Society, 138, 878–888, 2012.

Solomon, S., Portmann, R. W., Garcia, R. R., Thomason, L. W., Poole, L. R., and McCormick, M. P.: The role of aerosol variations in anthropogenic ozone depletion at northern midlatitudes, Journal of Geophysical Research: Atmospheres, 101, 6713–6727, doi:10.1029/95JD03353, http://dx.doi.org/10.1029/95JD03353, 1996.

Soukharev, B. E. and Hood, L. L.: Solar cycle variation of stratospheric ozone: Multiple regression analysis of long-term satellite data sets and comparisons with models, Journal of Geophysical Research: Atmospheres, 111, 20 314, 2006.

Thejll, P.and Schmith, T.: Limitations on regression analysis due to serially correlated residuals: Application to climate reconstruction from proxies, Journal of geophysical research, 110, D18 103, 2005.

van Loon, H. and Labitzke, K.: The Influence of the 11-year Solar Cycle on the Stratosphere Below 30 km: a Review, Space Science Reviews, 94, 259–278, doi:10.1023/A:1026731625713, http://dx.doi.org/10.1023/A%3A1026731625713, 2000.

van Loon, H. and Meehl, G. A.: The response in the Pacific to the Sun's decadal peaks and contrasts to cold events in the Southern Oscillation, Journal of Atmospheric and Solar-Terrestrial Physics, 70, 1046–1055, 2008.

van Loon, H., Meehl, G., and Shea, D.: The effect of the decadal solar oscillation in the Pacific troposphere in northern winter, J. Geophys. Res, 112, D02 108, 2007.

Walter, A. and Schönwiese, C. D.: Nonlinear statistical attribution and detection of anthropogenic climate change using a simulated annealing algorithm, Theoretical and Applied Climatology, 76, 1–12, doi:10.1007/s00704-003-0008-5, http://link.springer.com/10.1007/s00704-003-0008-5, 2003.

(a) MERRA
(b) ERA-Interim
(c) JRA-55
(d)
(e)
(f)
(g)
(h)
(i)
(j)
(k)
t
u
h
o3
Pressure [hPa]
Height [km]
Latitude [deg]
0.1
1
10
100
60
50
40
30
20
-90
0
90

Figure 1. The annually averaged response of the solar signal in the MERRA, ERA-Interim and JRA-55 zonal-mean temperature t (a)-(c), unit: [K], contour levels: $\mathbf{0}, \pm 0.25, \pm 0.5, \pm 1, \pm 2, \pm 5, \pm 10, \pm 15, \pm 30$; zonal wind u (d)-(f), unit: [m/s], contour levels: $\mathbf{0}, \pm 1, \pm 2, \pm 5, \pm 10, \pm 15, \pm 30$; geopotential height h (g)-(i), unit: [gpm]~~[m]~~[ales](r4,tc5), contour levels: $\mathbf{0}, \pm 10, \pm 20, \pm 50, \pm 100, \pm 150$; and ozone mixing ratio $o3$ (j)-(k), unit: percentage change per annual mean, contour levels: $\mathbf{0}, \pm 1, \pm 2, \pm 5, \pm 10$. The response is expressed as a regression coefficient RC (corresponding units per S_{max} minus S_{min}). The statistical significance of the scalar fields was computed by a t-test. Red and yellow areas indicate p-values < 0.05 and 0.01.

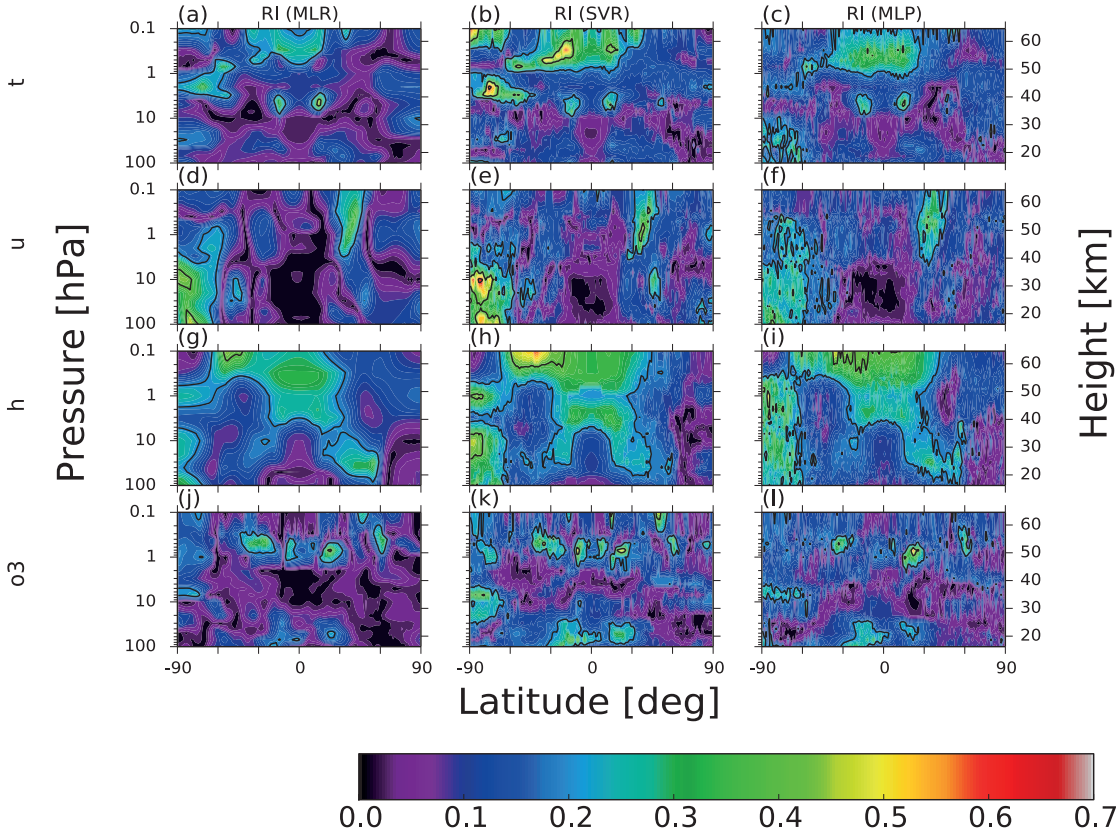

Figure 2. The annually averaged response of the solar signal in the MERRA zonal-mean temperature t (a)-(c), unit: [K]; zonal wind u (d)-(f), unit: [m/s]; geopotential height h (g)-(i), unit: [gpm]~~[m]~~[ales](r4,tc5); and ozone mixing ratio $o3$ (j)-(l), unit: percentage change per annual mean. The response is expressed as a relative impact RI approach. The relative impact was modeled by MLR, SVR and MLP techniques. The black contour levels in the RI plots are 0.2, 0.4, 0.8 and 1.0.

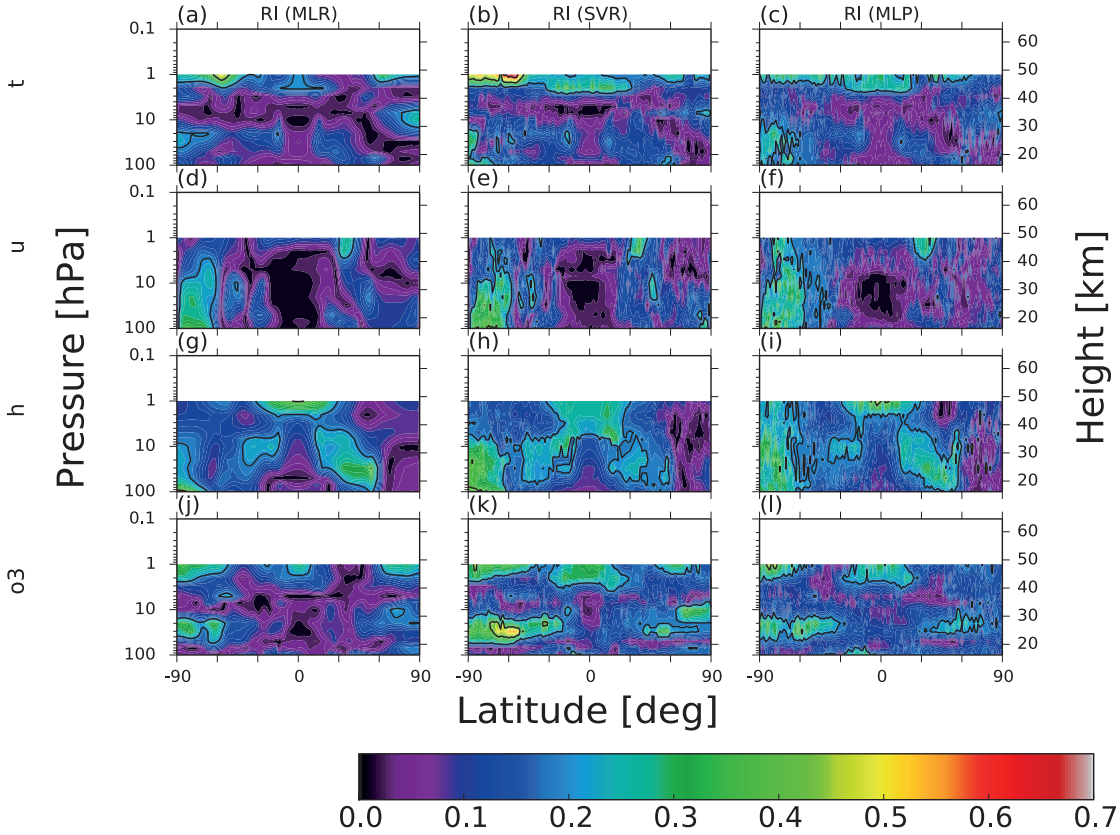

Figure 3. The annually averaged response of the solar signal in the ERA-Interim zonal-mean temperature t (a)-(c), unit: [K]; zonal wind u (d)-(f), unit: [m/s]; geopotential height h (g)-(i), unit: [gpm]~~[m]~~[ales](r4,tc5); and ozone mixing ratio $o3$ (j)-(l), unit: percentage change per annual mean. The response is expressed as a relative impact RI approach. The relative impact was modeled by MLR, SVR and MLP techniques. The black contour levels in the RI plots are 0.2, 0.4, 0.8 and 1.0.

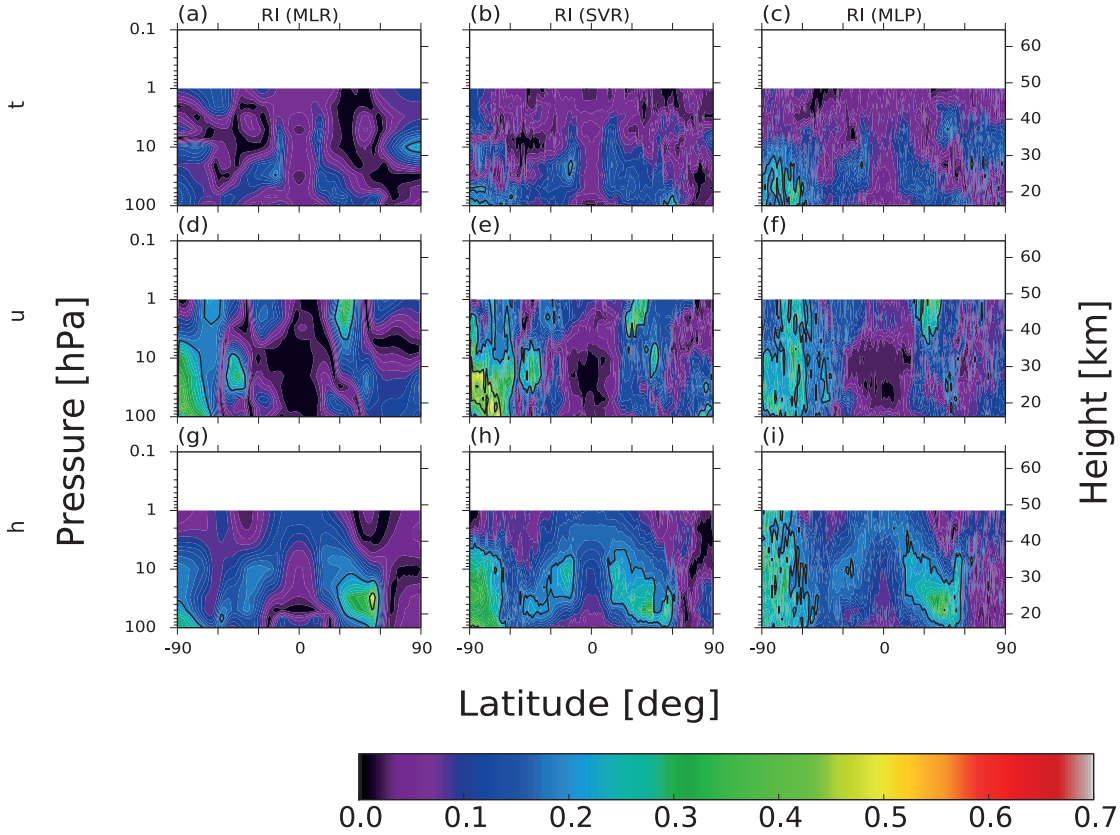

Figure 4. The annually averaged response of the solar signal in the JRA-55 zonal-mean temperature t (a)-(c), unit: [K]; zonal wind u (d)-(f), unit: [m/s]; geopotential height h (g)-(i), unit: [gpm]~~[m]~~[ales](r4,tc5); and ozone mixing ratio $o3$ (j)-(l), unit: percentage change per annual mean. The response is expressed as a relative impact RI approach. The relative impact was modeled by MLR, SVR and MLP techniques. The black contour levels in the RI plots are 0.2, 0.4, 0.8 and 1.0.

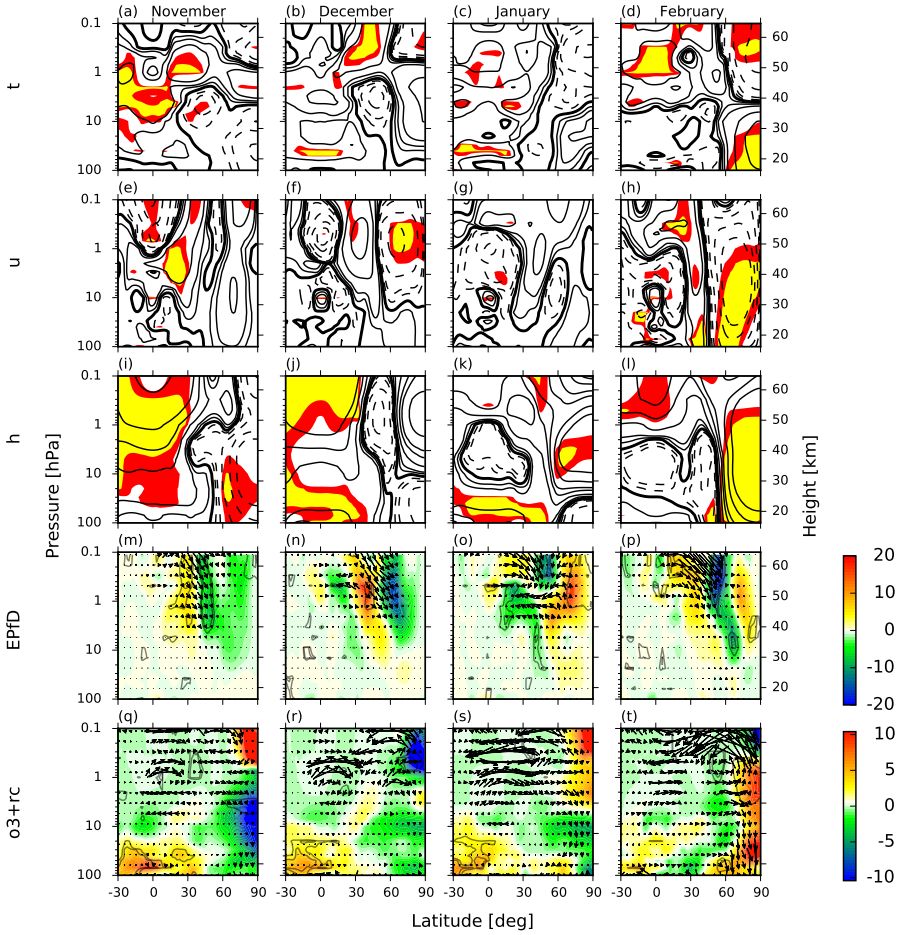
(a) November
(b) December
(c) January
(d) February
t
u
h
EPfD
o3+rc
Pressure [hPa]
Height [km]
Latitude [deg]
0.1
1
10
100
20
30
40
50
60
-30
0
30
60
90
20
10
0
-10
-20
10
5
0
-5
-10

Figure 5. The monthly averaged response of the solar signal in the MERRA zonal-mean temperature t (a)-(d), unit: [K], contour levels: $\mathbf{0}, \pm 0.5, \pm 1, \pm 2, \pm 5, \pm 10, \pm 15, \pm 30$; zonal wind u (e)-(h), unit: [m/s], contour levels: $\mathbf{0}, \pm 1, \pm 2, \pm 5, \pm 10, \pm 15, \pm 30$; geopotential height h (j)-(l), unit: [gpm][~~m~~]$^{\text{ales}}$(r4,tc5), contour levels: $\mathbf{0}, \pm 10, \pm 20, \pm 50, \pm 100, \pm 150, \pm 300$; EP flux divergence $EPfD$ (m)-(p), unit: [m/s/day]; together with EP flux vectors scaled by the inverse of the pressure, unit: [kg/s^2]; and ozone mixing ratio, unit: percentage change per monthly mean; with residual circulation $o3{+}rc$ (q)-(t), units: [m/s; 10^{-3}Pa/s] during northern hemispheric winter. The response is expressed as a regression coefficient (corresponding units per S_{max} minus S_{min}). The statistical significance of the scalar fields was computed by a t-test. Red and yellow areas in Figs. (a)-(h) and grey contours in Figs. (i)-(p) indicate p-values of < 0.05 and 0.01 respectively.

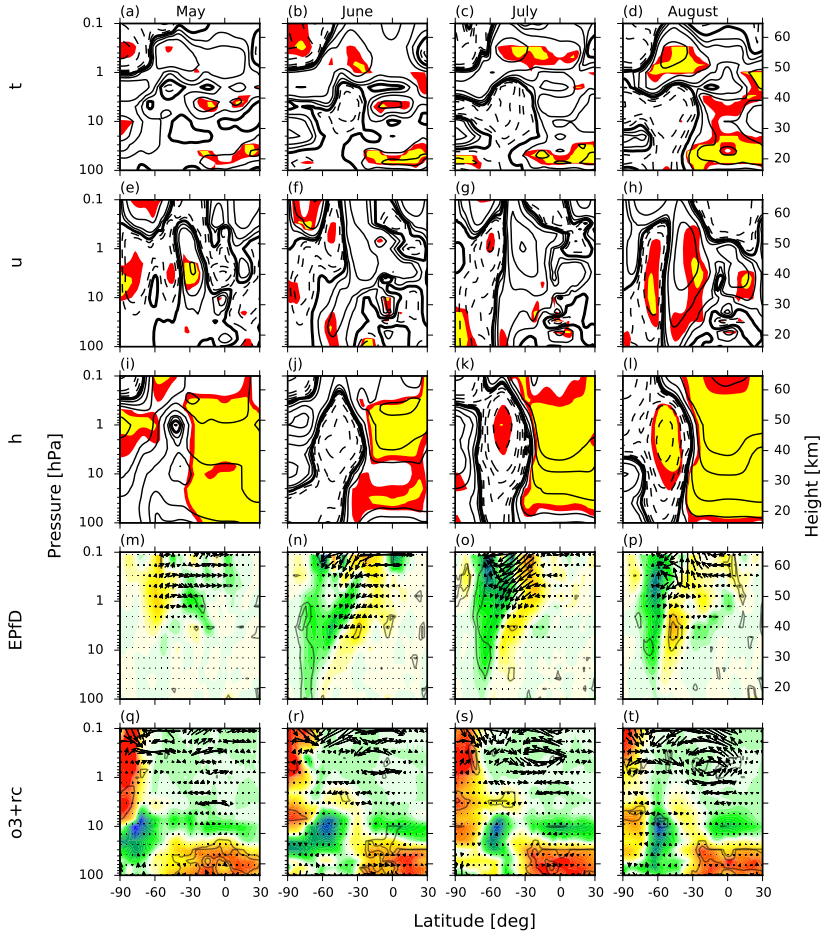
(a) May
(b) June
(c) July
(d) August
t
u
h
EPfD
o3+rc
Pressure [hPa]
Height [km]
Latitude [deg]

Figure 6. The monthly averaged response of the solar signal in the MERRA zonal-mean temperature t (a)-(d), unit: [K], contour levels: $\mathbf{0}, \pm 0.5, \pm 1, \pm 2, \pm 5, \pm 10, \pm 15, \pm 30$; zonal wind u (e)-(h), unit: [m/s], contour levels: $\mathbf{0}, \pm 1, \pm 2, \pm 5, \pm 10, \pm 15, \pm 30$; geopotential height h (j)-(l), unit: [gpm][~~m~~]$^{\text{ales}}$(r4,tc5), contour levels: $\mathbf{0}, \pm 10, \pm 20, \pm 50, \pm 100, \pm 150, \pm 300$; EP flux divergence $EPfD$ (m)-(p), unit: [m/s/day]; together with EP flux vectors scaled by the inverse of the pressure, unit: [kg/s^2]; and ozone mixing ratio, unit: percentage change per monthly mean; with residual circulation $o3{+}rc$ (q)-(t), units: [m/s; 10^{-3}Pa/s] during southern hemispheric winter. The response is expressed as a regression coefficient (corresponding units per S_{max} minus S_{min}). The statistical significance of the scalar fields was computed by a t-test. Red and yellow areas in Figs. (a)-(h) and grey contours in Figs. (i)-(p) indicate p-values of < 0.05 and 0.01 respectively.

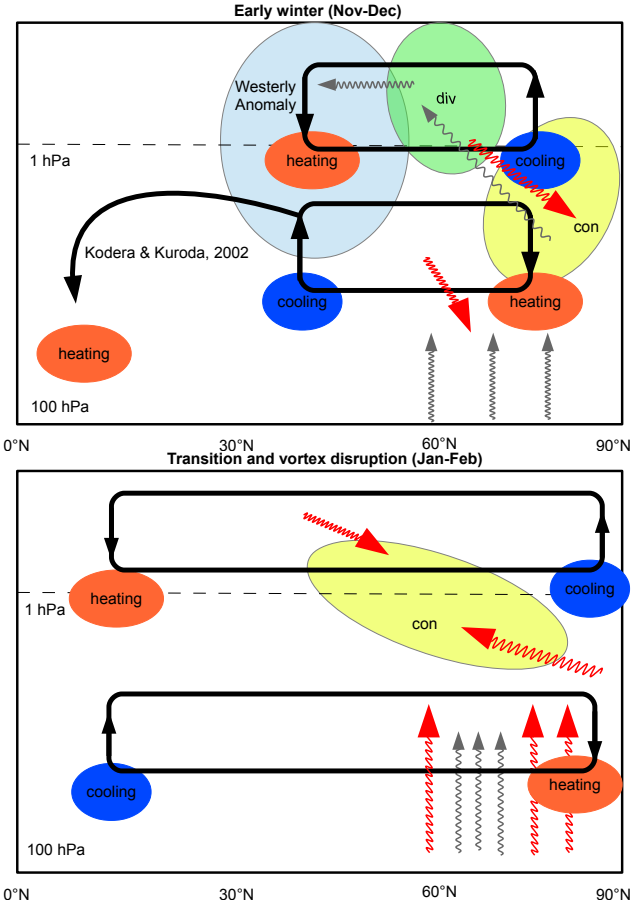
Early winter (Nov-Dec)
Westerly
Anomaly
div
1 hPa
heating
cooling
con
Kodera & Kuroda, 2002
cooling
heating
heating
100 hPa
0°N
30°N
60°N
90°N
Transition and vortex disruption (Jan-Feb)
heating
cooling
1 hPa
con
cooling
heating
100 hPa
0°N
30°N
60°N
90°N

Figure 7. Solar cycle modulation of the winter circulation: schema of the related mechanisms. The upper and lower figure show early and later winter respectively. The heating and cooling anomalies are drawn with red and blue boxes. The EP flux divergence and convergence are drawn with green and yellow boxes. The wave propagation anomaly is expressed as a wavy red arrow in contrast to the climatological average drawn by a wavy grey arrow. The induced residual circulation according to the quasi-geostrophic approximation is highlighted by the bold black lines.